Military Technical College
Kobry El-Kobbah,
Cairo, Egypt

14th International Conference on Applied Mechanics and Mechanical Engineering.

Film cooling performance of shaped hole over vane with flow visualization

By

T. Elnady*, W.Saleh*, I. Hassan*, L. Kadem*, T.Lucas**

Abstract:

The cooling performance of a shaped hole is investigated experimentally using a two-dimensional turbine vane cascade. The test section is designed to match Mach numbers, Reynolds numbers, pressure distributions, passage mass flow rates, boundary layer development, streamline curvature, and physical dimensions of turbine airfoils in operating gas turbine engines for industrial power generation. The test section walls are made of acrylic for the optical measurements with inlet cross section area of 10 cm by 5.4 cm. One row of laid-back fan-shaped axially-oriented cooling holes is located on the pressure side. The main stream Reynolds number based on the axial chord is 1.4E5 and inlet Mach number is 0.16. The local distributions of the heat transfer coefficient and film cooling effectiveness is obtained using a transient Thermochromic Liquid Crystal (TLC) technique for four different blowing ratios. The effectiveness of the shaped holes increases by the increase of the blowing ratio with a slight reduction on the heat transfer enhancement. The nature of the flow interaction between jet and mainstream is clarified using Particle Image Velocimetry (PIV) to support the heat transfer findings.

Keywords:

Gas turbine, film cooling, TLC and PIV

* Concordia University, Montreal, Canada
** Pratt & Whitney Canada.

1. Introduction:

With an elevated importance on environmental sustainability and depletion in fossil fuel resources around the world, it has become increasingly necessary to improve the efficiency and hence increase the power/weight ratio for the next generation of gas turbines. The most feasible way to do this is by increasing the temperature of the combustion products; however, this is limited by the thermal strength of the air passage materials. Film cooling is one of the cooling techniques that has been used to increase the cooling capacity in gas turbines, and is done by injecting a relatively cold flow to protect the heated surface. Many studies have investigated the cooling performance of film cooling on a flat plate with different hole geometries under various working conditions. For example, Jubran and Maiteh (1999) focused on two geometrical parameters, the compound angle of the hole exit, and the relative position between two successive rows. Yu et al. (2002) compared the cooling performance for cylindrical, fan-shaped and fan-shaped laid-back axially oriented film cooling holes using TLC and supported his findings through flow visualization. Bernsdorf et al. (2006) investigated the flow interaction between the standard cylindrical jet and the mainstream flows from a flat plate using PIV.

The flow physics on a highly curved surface, such as an actual turbine airfoil, differ from the flow physics on a flat surface. Therefore, several research studies have been conducted to investigate the film cooling performance over actual turbine airfoil coupled with multiple cooling row interactions. For example, Shuye T. et al. (2001) studied the effect of hole shape on the blade surface. Dittmar et al. (2003) conducted a similar study on the vane surface. Luzeng and Moon (2007) investigate the effect of hole location on cooling performance at the pressure side of a stator vane. Justin et al. (2008) studied the hole orientation using two different hole geometries. The purpose of this research is to measure the cooling performance of the laid-back fan-shaped hole on the pressure side of a gas turbine stator in terms of cooling effectiveness and heat transfer coefficient. The second objective is to support and explain the heat transfer findings by visualizing the interaction between the jet and the main stream using Particle Image Velocimetry (PIV).

2. Experimental setup:

A wind tunnel was recently established at Concordia University to investigate the film cooling performance in gas turbines. The test facility consists of both mechanical and electronic systems, and was well documented by Ghorab (2009) for a flat plate investigation. In the current study, modifications to the test facility were done in order to investigate the film cooling performance of a scaled airfoil using the two dimensional cascade. This cascade, illustrated in Figure 1, provides similar flow passages that matched the operating flow conditions (M, Re, pressure distribution) around a scaled vane used in industrial power generation. An additional adaptor, with an inlet cross-sectional area of 27.5 cm by 12 cm, installed on the main flow line, upstream of the cascade, to reduce the tunnel cross-sectional area to 9.5 cm by 5.1 cm. A duct of the same cross section, and 150 cm in length, used to convey a fully developed mainstream to the airfoil test sections. A small plenum with an

internal dimension 7×2×2cm, assembled at the bottom of the base part of the test section to feed the airfoil with the secondary flow. Fast acting 3-way solenoid valves routed the secondary flow through a bypass until steady state conditions were achieved. A thermocouple and a pressure sensor are inserted in the plenum to record the static temperature and pressure of the jet before being delivered to the airfoil.

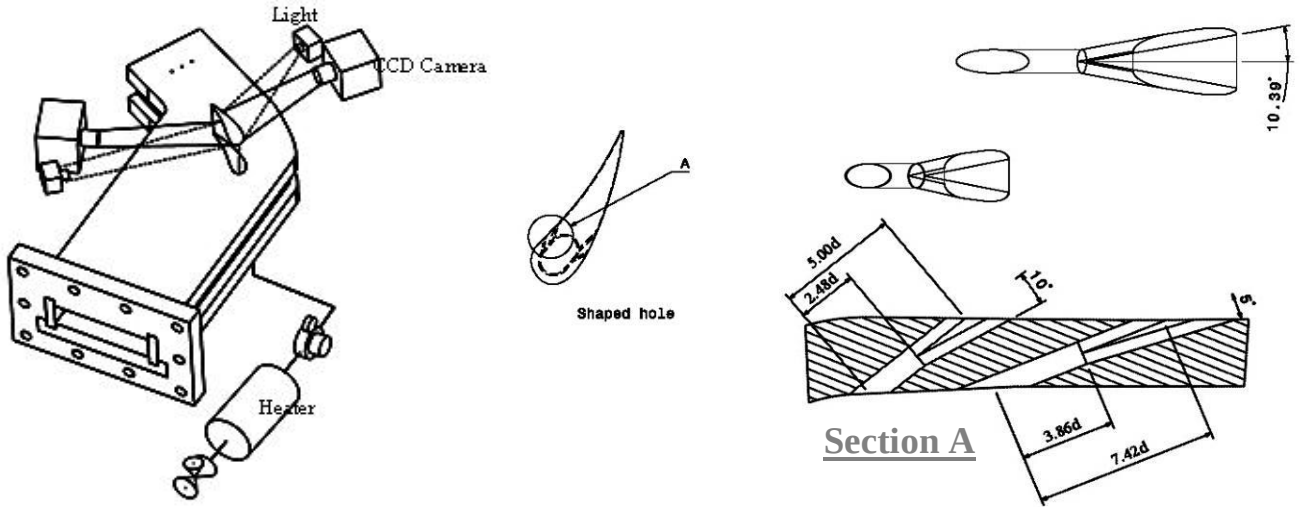

Figure (1): *Vane cascade and hole geometry*

The pressure distribution around the airfoil is recorded using a Scanivalve pressure transducer. The pressure taps on the airfoil surface are connected to the pressure scanner channels using Urethane flexible tubing with 1/16" inside diameter. The differential pressure between the reference point and the measured points is recorded using DSA Link 3.03. Fourteen pressure taps are drilled along the midspan, seven taps on the pressure side, six at the suction side, and a pressure tap on the leading edge just at the stagnant point. A tap located at the suction side of the airfoil, close to the leading edge, has a mean pressure value between all other tap readings, so it is selected to be the reference point. The readings of all pressure taps are referred to this reference tap reading, and a tap on the pressure scanner is subjected to atmospheric pressure to get the absolute value for each point. During each blow down test, the total pressure and Reynolds number at the test section inlet are maintained in a continuous and steady fashion for intervals of up to 60 seconds. The pressure at each tap is recorded at a rate of 20 Hz and averaged through the running time period. The inlet pressure to the test section is measured one axial chord length upstream of the vane leading edge.

Seven laid-back fan-shaped holes are arranged on one row on the pressure side at 28% of the axial chord. The holes are inclined with 22^{o} angle with the streamwise direction with a spanwise spacing of 4.5d, as shown in Figure 1. Another vane with similar hole geometry, but with a standard cylindrical exit, was manufactured for comparison purposes. Each vane is manufactured with a groove of 0.254 mm depth downstream the cooling row. This depth is equal to the TLC sheet thickness in order to allow the mapping of the temperature distribution over the vane surface without disturbing the development of the boundary layer.

A uniform rectangular grid, 5 mm spacing, is drawn on the vane surface to account for the curved surface of the vane. The actual distance between grid lines are digitally measured, as a number of pixels, at different locations along the vane surface and correlated to the actual linear distance. Thermochromatic Liquid Crystal (TLC) are used to map the temperature

distribution along both sides of the vane surface. A special vane is designed for performing the TLC calibration process to account for the curvature effect. The calibration vane is manufactured with a special groove of 5cm×5cm×0.36mm in dimensions to contain both the heater and the TLC sheet. The heater with a maximum power output of 0.4W/cm^2 is used to apply a uniform heat flux to the TLC sheet during the calibration process to achieve the same lighting and camera settings for both calibration and experimental running processes. The heater is fed through a DC regulator to ensure infinitesimal power steps followed by steady state duration.

Particle Image Velocimetry has the ability to measure two-dimensional or three-dimensional fluid velocity fields. In this technique, the fluid under investigation is seeded with tracer particles that follow the flow field. The seeding generator produces tiny droplets of Olive oil with mean diameters of approximately 1 μm by pressurized air. The particles are illuminated using a pulsed laser having a capacity of 120 mJ/pulse at a 532 nm wavelength and a maximum pulse rate of 5 Hz. Optics convert the single beam output from the laser head into a light sheet. A pair of digital output CCD cameras, with 1344×1024 pixel resolution, is used to capture the particle displacement with Nikon objective lens for providing focal and illumination adjustments. A frame grabber card records the images in conjunction with a timer board to synchronize the image capturing and laser pulses. A Dell Precision Workstation with two 3.60 GHz processors, 4 GB of RAM, and two 250 GB 7200 RPM hard disks handles the large data processing requirement. The commercial Flow Manager software performed the necessary correlation functions, filtering, and statistical analysis to generate the resolved velocity fields.

Spatial calibration was done by using a calibration target (an accurate ruler with a 0.1 mm reading). The calibration target was used to identify the investigated planes. The region of interest size was 15 mm x 11.5 mm and the picture size in pixels was 1024x1344 pixels. So the spatial resolution was around 89 pixels per mm. A traverse is used to move the laser and the camera through different investigated planes keeping the same relative distance between the laser sheet and the focus of the camera.

3. Data reduction:

A set of images is captured at different power inputs given that a steady state temperature reading is achieved after each power step. This set of images, in conjunction with the surface temperature recorded by two thermocouples at two different positions, is used to map the temperature distribution over the vane surface in the running experiment. During each running test a set of images is captured for 60 seconds at a rate of 5Hz for a total of 300 images of 1024x768 pixels. A region of the upper three holes is selected, to minimize the conduction effect, and the color contours in each image are interpreted to a temperature contour on a basis of a 1x1 pixel Region Of Interest (ROI).

The one-dimensional transient heat conduction through a semi-infinite solid is assumed to determine the local heat transfer coefficient and cooling effectiveness. The unsteady heat conduction equation for one dimensional heat conduction into a semi-infinite solid is given as:

$$\rho C_p \frac{\partial T}{\partial t} = \frac{\partial}{\partial x}\left(K \frac{\partial T}{\partial x} \right) \tag{1}$$

with the initial and boundary conditions

$$h\left(T_w - T_f\right) = -K\frac{\partial T}{\partial x} \tag{2}$$

t=0, $T=T_i$,

x=0

x=∞, $T= T_i$

$$\frac{T_w - T_i}{T_f - T_i} = 1 - \exp\left(\frac{h^2 \alpha t}{k^2}\right) erfc\left(\frac{h\sqrt{\alpha t}}{k}\right) \tag{3}$$

Ping-Hei et al. (2001) gave the solution for Eq. (1) with boundary conditions in Eq. (2) to be:

The initial temperature, T_i, of the surface as well as the mainstream temperature, T_m, will be measured by using a thermocouple. The film temperature, T_f, can be calculated as a function of coolant temperature, T_c, mean temperature, and film cooling effectiveness as follows

$$\eta = \frac{\left(T_f - T_m\right)}{\left(T_c - T_m\right)} \tag{4}$$

Each airfoil shape has its own streamline that affects the heat transfer over its surface; in addition, the same airfoil itself has different streamline expansions on both the pressure and suction sides. Therefore, the most proper way to present the heat transfer changes on the airfoil surface is by normalizing the heat transfer coefficient of film cooling (h_f) to the heat transfer coefficient without film cooling (h_o) in order to present the actual effect of parameters changing on the heat transfer. The calibration vane can be used for measuring the heat transfer coefficient without film cooling over the vane surface. The mainstream flows over the vane by applying a constant heat flux using the electric heater. When achieving a steady state, the CCD camera captures an image of the vane presenting the corresponding temperature contours over the TLC material. The heat transfer coefficient without film cooling can be obtained by applying Eq. (5).

$$h_o = q/(T_w - T_m) \tag{5}$$

The heat losses (q_{loss}) in terms of conduction, electric, and radiation losses are estimated to be fifteen percent of the total heat load applied by the heater (q_{elec}), hence $q=q_{elec} - q_{loss}$, or $q = 0.85\ q_{elec}$.

Uncertainty analysis is based on 95 percent confidence levels, and determined using procedure described by Kline and McClintock (1953) and by Moffat. (1988) Mach number uncertainty is 0.002, Temperature is 0.2^oC, pressure is 0.2kPa, and the spatial resolution with TLC imaging is 0.1 mm. The uncertainty in determining the exact locations of thermocouples

with respect to local position of each pixel in the calibration process is 0.4°C. These uncertainty leads to 0.018 in adiabatic effectiveness, about ± 9 percent for a nominal effectiveness of 0.2. The uncertainty in heat transfer coefficient is found to be 33 W/m^{2}K, about 9.5 % of averaged span-wise heat transfer coefficient value of 350 W/m^{2}K

4. Flow characteristics and heat transfer base line:

During each test, the inlet pressure, one chord upstream of the vane leading edge, is maintained constant at 93 kPa. This corresponds to 0.25 exit free stream Mach number and 2x10^5 exit Reynolds number based on the axial chord. Inlet uniformity is measured at three different pitch-wise locations, one chord upstream from the vane, and it shows high uniformity for static pressure varying by less than 1 percent of the mean value. The static pressure is measured at fourteen different locations over both sides of the vane. By assuming compressible flow with isentropic flow relations the corresponding Mach number at each location is obtained and plotted on Figure 2.

Mach number distributions employed in this study are subsonic on both pressure and suction sides. The pressure expansion yields a corresponding drop in the local temperature along the vane surface. This temperature drop affects the cooling effectiveness as the mainstream temperature changes at different positions along the vane midspan. Mach number and temperature distributions of the main stream have been determined from the isentropic gas laws using the pressure readings. The vane in this study shows a higher heat transfer at x/C_x =0.2, with rapid decay up to x/C_x =0.3 in the transition region. The heat transfer is then increased with the surface distance as the boundary layer is thickening in the fully turbulent region.

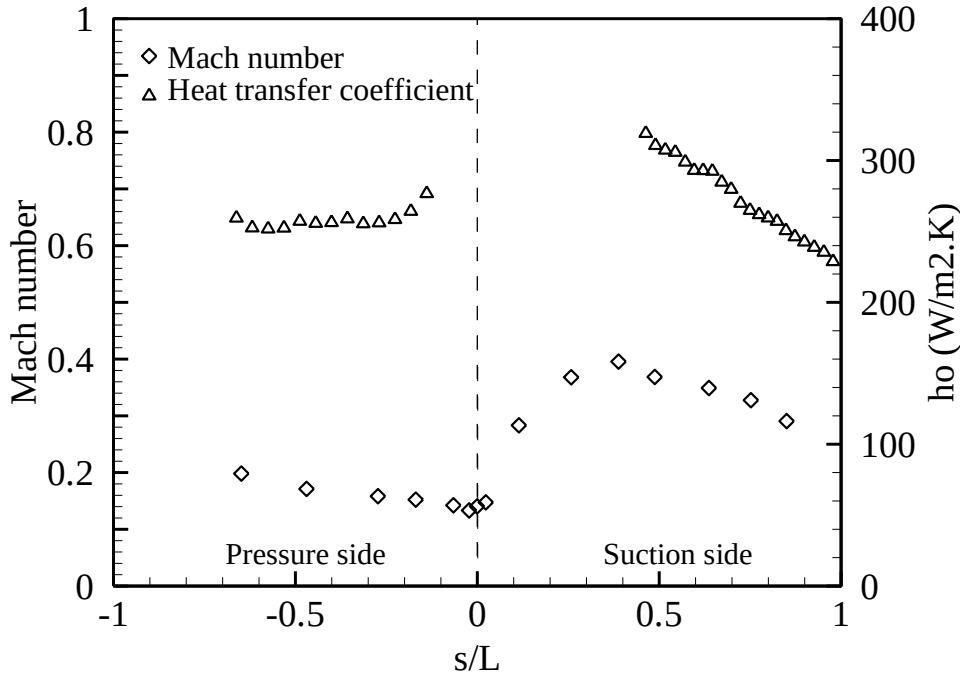

Figure (2): *Vane Mach number distribution*

5. Average spanwise cooling performance:

This study compares the cooling performance of two different hole exit shapes, standard cylindrical and fan-shaped, that have the same base diameter. This comparison is performed based on the same coolant amount being delivered to both schemes. Due to the expanded area of the shaped exit, its hydraulic diameter is larger than the corresponding one of a standard cylindrical exit. This difference altered between both rows because of the difference in curvature ratio (d/R). Based on this comparison, any blowing ratio mentioned with the shaped exit is referred to the corresponding blowing ratio for the cylindrical scheme that gives the same coolant amount. This method is selected to reveal the exact effect of hole exit shape on the jet expansion and its reflection on the cooling performance of the investigated shape. The surface distances for both shapes are referred to the trailing edge of the cylindrical exit. The color contours of the TLC sheet is interpreted to temperature contours and hence to cooling performance contours. The performance is quantified in terms of cooling effectiveness and normalized heat transfer coefficient. The spanwise values of the effectiveness are averaged and presented along the streamwise direction in Figure 3a.

For the cylindrical exit the effectiveness decreases with the blowing ratio giving the maximum effectiveness at BR = 1. This observation means that the jet lift-off starts at this blowing ratio, or may be lower as lower BR are not included in this study. Contrary to the cylindrical exit, the shaped exit gives better performance with increasing the blowing ratio. At low blowing ratio, BR = 1, the jet has low cooling capacity and quickly dilutes in the mainstream causing lower effectiveness for a short distance. By increasing the blowing ratio, the coolant amount increases, giving higher effectiveness, however, the coolants mixed with the mainstream lose its cooling capacity. These findings emphasize the expected improvement on the cooling performance by using shaped holes compared with the standard cylindrical holes. The cylindrical exits allows higher jet velocity at point of interaction causing severe diffusion on the mainstream. This diffusion is called jet lift-off and it increases by the increase of the blowing ratio, causing lower effectiveness. The expansion in the hole exit decreases the jet velocity and hence decreases the jet momentum allowing the mainstream momentum to force the jet close to the surface.

The local heat transfer coefficient of the injection is divided by each corresponding heat transfer coefficient without film cooling and averaged on the spanwise direction and presented in Figure 3b. In the standard cylindrical injection, the jet introduces to the turbulent boundary layer and increases its thickness causing heat transfer enhancement. However, the fluctuated particles on the main stream rapidly diffused through the jet causing a mixing between both streams and a decrease in the heat transfer enhancement. The jet is then reattached to the surface causing the lowest heat transfer enhancement, nearly at x/d = 14. The higher blowing ratio has the highest h/ho, however, the difference between all blowing ratios effects is quite well within the measurement uncertainty. The shaped exit presents better heat transfer enhancement, near downstream the hole, due to the expanded exit and it provides longer surface distance with the better heat transfer enhancement. The shaped hole shows, similar to the cylindrical exit, highest h/ho values at the higher blowing ratios with tendency to unity far downstream. The flow visualization shows more explanation for the special interaction between both flows.

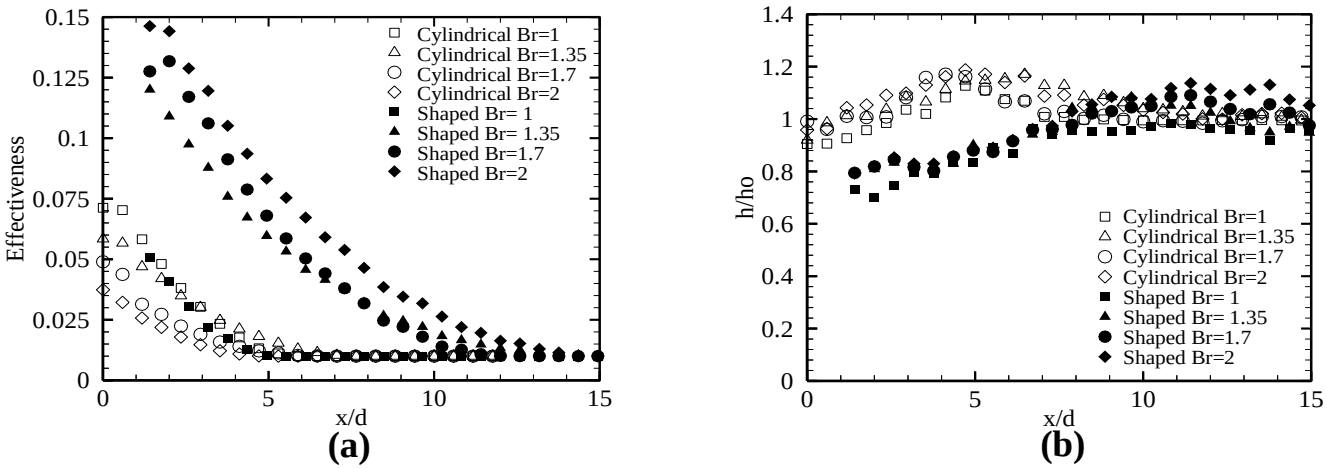

Figure (3): *Cooling performance a) effectiveness b) heat transfer enhancement*

6. Velocity field:

Two sets of results are presented here; the trace of the secondary flow by seeding the secondary flow only, and the trace of main flow by seeding the mainstream only. Figure (4a) shows the velocity development inside the boundary layer at different x/d for the case of Br = 1.35. The velocity profile development gives an indication about the effect of the blowing ratio on the secondary flow penetration inside the main flow. Figure (4b) shows the velocity variation for Br = 0.0, 1.0, 1.35, 1.7, and 2.0 inside the boundary layer at x/d = 3.0. The points located inside the dashed rectangle have the same y/d and they show the jet effect on the boundary layer by changing the blowing ratio. Up to y/d = 0.55 the most effected main stream velocity at Br = 2.0. This can be explained by the high velocity of the secondary flow creates a concentrated jet and its effect reaches to y/d = 0.55. From y/d = 0.7 to y/d = 1.0 the most effected main stream velocity at Br = 1.7. The reason for this is that the relatively high BR = 1.7 penetrates more into the main stream and its effect reaches to y/d = 1.0. This can be explained by the jet lift off of the secondary flow then it tends toward the surface again with less effect on the main velocity profile.

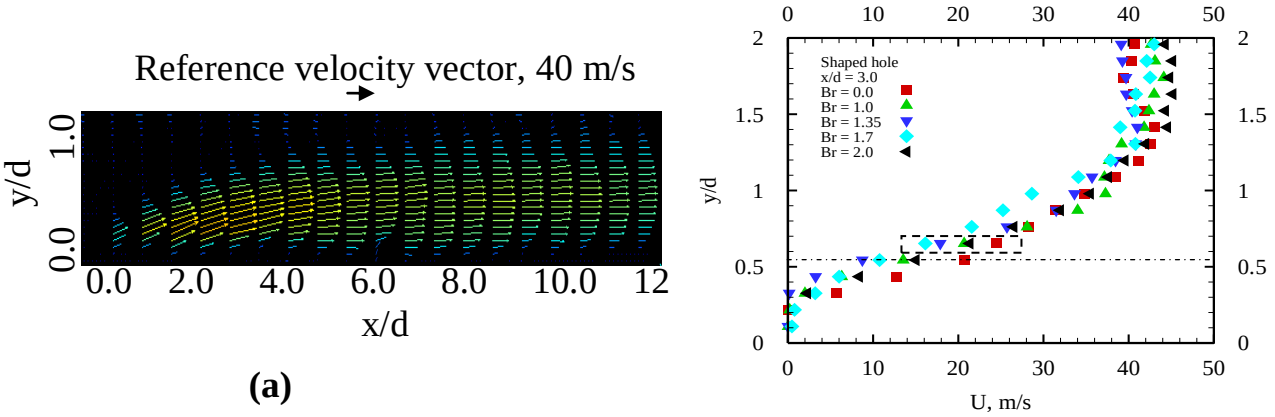

Figure (4): *Jet velocity profile a) attached jet b) boundary layer development*

7. Conclusions:

This study aims to investigate the cooling performance of the shaped hole on the actual surface of the gas turbine vane using a two-dimensional cascade. Two techniques are used; TLC to map the temperature distribution and hence the cooling performance, and PIV to draw the velocity field and hence explain the interaction between the jet and the mainstream. The shaped holes provide better cooling effectiveness compared with the cylindrical holes because of its expanded exit. This expansion reduces the jet momentum by decreasing its velocity. By decreasing the jet momentum, the jet lift-off is decreased and the mainstream dominates the jet causing it more attached to the vane surface. The shaped holes also have the advantage of more jet lateral spreading that provides more uniform coverage and hence uniform thermal stresses on the airfoil. Moreover, the shaped holes allow using higher blowing ratios that have more coolant amount to extend the cooling effect for farther distances on the surface.

References:

[1] Dittmar J., Schulz A., Wittig S.; "*Assessment of various film cooling configurations including shaped and compound angle holes based on large scale experiments*", Proceeding of ASME Conference, Paper No. GT-2003-30176, 2003.

[2] Bernsdorf S., Rose M. G., Abhari R. S.;"*Modeleing of film cooling-Part I:Experimental Study of Flow Structure*"; J. of Turbomachinery, Vol.128, P141-149

[3] Ghorab G. M.; *Experimental Investigation of Advanced Film Cooling Schemes for a Gas Turbine Blade*" PhD thesis, Concordia University, 2009.

[4] Jubran B.A., Maiteh B.Y.;" *Film cooling and heat transfer from a combination of two rows of simple and/or compound angle holes in inline and/or staggered configuration*" Journal of Heat and Mass Transfer, vol. 34, p495-502, 1995.

[5] Justin C., Ligrangi P., Sri S., Terry L.; "*Suction side gill-region film cooling: effects of hole shape and orientation on adiabatic effectiveness and heat transfer coefficient*"; Proceeding of ASME Turbo Expo, paper no. GT2008-50798, 2008.

[6] Luzeng Z. and Hee-K. M.; "*Turbine blade film cooling study- the efficiency of film hole location on the pressure side*"; Proceeding of ASME TurboExpo, paper no. GT2007-27546, 2007.

[7] Ping-Hei C., Ai D., Ding P.P., "*Selection criterion of injection temperature pair for transient liquid crystal thermography on film cooling measurements*" International Journal of Heat and Mass Transfer, vol. 44, n 7, p 1389-1399, 2001

[8] Shuye T., Han J.C., Philip E. P.; "*Effect of film hole shape on turbine-blade heat-transfer coefficient distribution*"; Journal of Turbomachinery and Heat transfer, vol. 15, No.3, p 249-256, 2001.

[9] Yu Y., Yen C.H., Shih T.I.P., Chyu M.K., Gogineni S., "*Film cooling effectiveness and heat transfer coefficient distributions around diffusion shaped holes*"; Journal of Heat Transfer, vol. 124, n 5, p 820-827, 2002

Nomenclature:

C	true chord
C_p	specific heat capacity
C_x	axial chord
d	hole diameter
H	hue value
h	heat transfer coefficient with film cooling
h_o	heat transfer coefficient without film cooling
k	thermal conductivity
l	hole length
P	pitch (distance between two holes)
T	temperature
T_i	Initial temperature of the surface
t	time
v	velocity

Greek

α	thermal diffusivity
η	film cooling effectiveness
ρ	density

Subscripts

c	coolant
f	film
j	jet
m	main flow
w	wall (surface)

Acronyms

B.R.	Blowing Ratio [(ρ v)$_j$/(ρ v)$_m$]
P.R.	Pressure Ratio (p_j/p_m)
PIV	Particle Image Velocimetry
ROI	Region Of Interest
TLC	Thermochromic Liquid Crystal